J Appl Electrochem (2010) 40:967–980
DOI 10.1007/s10800-009-9966-3

ORIGINAL PAPER

Mathematical modeling of AC electroosmosis in microfluidic and nanofluidic chips using equilibrium and non-equilibrium approaches

Jiří Hrdlička · Petr Červenka · Michal Přibyl · Dalimil Šnita

Received: 9 December 2008 / Accepted: 2 July 2009 / Published online: 28 July 2009

Abstract AC electroosmotic micropumps are suggested to be powerful tools for electrolyte dosing in various micro- and nanofluidic systems. In this paper, we compare two modeling approaches for studying the AC electroosmosis in the following micro and nanochannel systems: (i) a traveling-wave AC pump with a spatially continuous wave of electric potential applied on a planar boundary, (ii) a traveling-wave AC pump with a wave of electric potential applied on a set of discrete planar electrodes, and (iii) an AC pump with a set of non-planar electrodes. The equilibrium approach is based on the use of capacitor–resistor boundary conditions for electric potential and the slip boundary conditions for velocity at electrode surfaces. The non-equilibrium approach uses the mathematical model based on the Poisson equation and the non-slip boundary conditions. We have observed discrepancies between the predictions given by the both models and then we have identified their possible reasons. The comparison of the equilibrium and non-equilibrium results further showed three important actualities: (a) how the equilibrium model overestimates or underestimates the net velocity, (b) how the velocity maxima in the frequency characteristics can be shifted, if the equilibrium model assumptions are not satisfied, (c) the parametric region where the equilibrium model is applicable. Because the data are obtained in a dimensionless form, they can be exploited for AC electroosmotic studies. We discuss the limitations of the equilibrium and non-equilibrium models and compare selected predictions with available experimental data.

J. Hrdlička · P. Červenka · M. Přibyl (✉) · D. Šnita
Department of Chemical Engineering, Institute of Chemical Technology, Prague, Technická 5, 166 28 Prague 6, Czech Republic
e-mail: Michal.Pribyl@vscht.cz; pribylm@vscht.cz

Keywords Electrokinetics · Microfluidics · Nanofluidics · AC electroosmosis · Traveling-wave · Mathematical modeling

List of symbols

A	Amplitude (V)
c	Concentration (mol m^{-3})
C_D	Capacitance of EDL (F m^{-2}) $C_D = \varepsilon/\lambda_D$
D	Diffusivity (2×10^{-9} m^2 s^{-1})
f	Frequency (s^{-1})
F	The Faraday constant (96,485 C mol^{-1})
g	Gap width (m) $g = x^L_{m+1} - x^R_m$
h	Electrode height (m)
H	Height of a periodic segment (m)
$\mathbf{J}$	Ion flux intensity (mol $m^{-2}s^{-1}$)
k	Wave number (m^{-1}) $k = 2\pi/L$
L	Length of a periodic segment (m)
L^e	Electrode width (m) $L^e = x^R_m - x^L_m$
n	Number of electrodes
n_{Fx}	Number of finite elements in the x-direction
n_{Fy}	Number of finite elements in the y-direction
$\mathbf{n}$	Normal unit vector
p	Pressure (Pa)
q	Electric charge density (C m^{-3})
R	Molar gas constant (8.314 J $K^{-1}mol^{-1}$)
t	Time (s)
$\mathbf{t}$	Tangential unit vector
T	Temperature (298.15 K)
T_t	Period of the electric signal (s) $T_t = f^{-1}$
v	Horizontal component of velocity (m s^{-1})
$\langle v \rangle$	Net velocity (m s^{-1})
$\mathbf{v}$	Velocity (m s^{-1})
w	Electric potential wave velocity (m s^{-1}) $w = L/T_t = \omega/k$

x Spatial coordinate (m)
y Spatial coordinate (m)

Greek symbols

α Phase of an AC signal
ε Electrolyte permitivity (6.9503×10^{-10} F m^{-1})
φ Electric potential (V)
η Dynamic viscosity (0.001 Pa s)
λ_D The Debye length (m) $\lambda_D^2 = \frac{\varepsilon D}{\sigma}$
ψ Complex electric potential (V)
ρ Density (1,000 kg m^{-3})
σ Specific conductivity (S m^{-1}) $\sigma = 2c_\circ D\frac{F^2}{RT}$
ω Angular frequency (s^{-1}) $\omega = 2\,\pi f$

Dimensionless criteria

Ra The Rayleigh number $\mathrm{Ra} = \frac{\varepsilon}{\eta D}\left(\frac{RT}{F}\right)^2 = 0.2294$
Sc The Schmidt number $\mathrm{Sc} = \frac{\eta}{\rho D} = 500$
$\tilde{\lambda}_D$ EDL simplex $\tilde{\lambda}_D = \lambda_D/L$

Superscripts

$*$ Complex conjugate
$\sim$ Dimensionless
$\wedge$ Time averaged
$+$ Cation
$-$ Anion
$\pm$ Either $^+$ or $^-$
e Electrode
L Left boundary of the electrode
R Right boundary of the electrode
C Center of the electrode

Subscripts

o Characteristic value
m Index of electrode
slip At the slip plane

1 Introduction

Ramos et al. studied the effects of a low amplitude AC electric field imposed on co-planar electrodes in a microchannel filled by aqueous electrolytes [1]. They observed the electrokinetic transport of a new kind above the microelectrodes for frequencies up to 500 kHz. In 2000, Ajdari proposed a design of AC electrokinetic micropumps based on arrays of asymmetric pairs of co-planar microelectrodes [2]. It was expected that the asymmetry will lead to a net flow of electrolytes. His predictions were verified by several experimental and theoretical works, e.g., [3–7]. In general, the authors used microelectrodes with characteristic dimensions from micrometers to tens of micrometers. The observed net flow velocity typically attained few hundreds of microns per second.

The AC electroosmotic flow is based on the same principles as the DC electroosmosis [8], i.e., on existence of the tangential coulombic force at a polarized solid phase. For example in the co-planar AC electroosmotic micropumps, the imposed electric field has the tangential and the normal components. The normal component induces the electrode polarization (capacitive charging). Then, the lateral component of the electric field forces the amassed electric charge to move along the electrodes. The most intensive tangential coulombic force was predicted and observed at electrode edges [9]. As the electric charge is formed by ions of a non-zero diameter, the moving ionic particles pull a surrounding liquid via the viscous forces. Combination of the coulombic, pressure and viscous forces in the liquid results in the formation of eddies above the electrodes that were experimentally observed by PIV techniques [4, 5]. The system asymmetry leads to an asymmetry of the eddies and to a non-zero net velocity.

We can recognize at least three different types of the AC electroosmotic micropumps according to the microelectrode arrangement: (i) micropumps with asymmetric co-planar electrodes (AM), (ii) micropumps with 3D or non-planar electrodes (3DM), and (iii) traveling-wave electroosmotic micropumps (TWM).

Bazant et al. theoretically predicted that the 3DM design will increase the electrolyte net velocity up to mm/s [10, 11]. Their theory arises from fact that the counter-rotating regions of fluid observed above the electrodes inhibit the net flow. Hence, the authors suggested using the 3DM pumps with asymmetric raised steps. In such arrangement, an electrolyte flows in a manner of "fluid conveyor belt" above the non-planar electrodes and the counter-rotating eddies are burrowed between adjacent electrodes. It has been experimentally verified that the net velocity can be increased at least by one order of magnitude with respect to the pure co-planar arrangement [12, 13].

The TWM pumps rely on either a traveling-wave electric potential applied to an array of microelectrodes or a spatio-temporally modulated surface potential on insulating microchannel walls [14–19]. In the most common arrangement, a harmonic traveling wave of electric potential is applied on a set of n co-planar or non-planar microelectrodes with the phase shift $360/n°$ between two adjacent electrodes.

The AM and 3DM systems usually use an interdigitated arrangement, e.g. [7]. Fabrication of the TWM pumps is more difficult due to topological reasons. However, it is possible to exploit a practical spiral design of microelectrodes [14].

The net flow velocity in AC micropump systems strongly depends on many parameters, e.g. [7, 13, 14, 20]: (i) electric field parameters (amplitude, frequency, phase shift), (ii) electrolyte parameters, and (iii) geometric properties. Thus the AC micropumps suffer from the same disadvantage as the DC electroosmotic systems—a high

sensitivity of the pumping performance to structural and operational parameters. However, the strong dependence of the net velocity on the applied voltage and frequency can be used for a simple control of the flow intensity and the flow direction [7, 19, 21]. The main advantage of the AC pumps is that only a low amplitude electric signal has to be applied on a microelectrode system. The amplitude usually does not exceed several Volts, which results in a substantial reduction of undesirable faradaic interactions on the electrode surfaces.

Mathematical models of AC electroosmosis have been developed. The computation domain is usually divided into the capacitor domains [vicinities of the polarized surfaces, where electric double layers (EDL) are formed] and the resistor domain (the electrolyte bulk). It is assumed that electric potential in an arbitrary point of the system can be represented by a product of a complex time-independent function and a time-dependent function (e.g., harmonic). Then, the boundary conditions for electric potential on the capacitor–resistor interfaces can be derived. However, these boundary conditions are valid only when a low voltage (amplitude <25 mV) is applied on the microelectrodes, i.e., the linearization of the Poisson–Boltzmann equation is justified [20]. When a higher voltage is applied, distributions of the ion concentration and the electric charge in a proximity of the electrodes are not linear functions of the voltage. Hence, the capacitance of the EDL capacitance can not be considered to be independent of the applied voltage in such case. Further, the Boltzmann distribution is valid only for systems in the thermodynamic equilibrium. The AC electroosmotic systems are rarely close to the equilibrium because of the intensive convection transport at the electrode surfaces. In spite of the mentioned limitations, the capacitor–resistor boundary conditions are used in the most of the reported analyses, e.g. [2, 5, 13, 19]. If the distribution of the electric potential at the capacitor–resistor interface is evaluated, then slip velocity boundary conditions can be expressed by the Helmholtz–Smoluchowski equation [8]. So, the transport (flow) problem is solved independently and only in the resistor domain represented by the electrolyte bulk.

Mathematical models relying on the above mentioned capacitor–resistor slip approximation [21–23], and more complex Poisson–Boltzmann models [24, 25] and non-equilibrium models [18, 26, 27] have been developed. The Poisson–Boltzmann approach allows analyzing model equation for voltages above the linearization limit, however, EDL is still considered to be in the thermodynamic equilibrium. The non-equilibrium models describe the electric potential distribution with the use of the Poisson equation and zero velocity is applied on solid surfaces. The models based on the Poisson equation should satisfactorily describe the behavior of the AC electroosmotic systems with non-equilibrated EDLs even if a higher voltage applied.

Kilic et al. [28] pointed out the fact that for higher applied voltages the classical Poisson–Boltzmann theory predicts an inadmissible increase of the ionic concentration at polarized surfaces. The concentration can not grow above a certain value in real ionic systems due to steric effects. The authors introduced a pseudo-diffusion term in the balances of ions and the electric charge [29]. The coefficient used in the pseudo-diffusion term is a function of the ionic concentration and rises to infinity when the steric limit is attained. Numerical analysis of an AC electroosmotic system, for which the steric effect were considered, was reported in [30]. The authors, for example, found that the model is able to predict flow reversals often observed in the AM systems.

In this paper, we will compare two approaches for modeling of the AC electroosmosis in selected microsystems: (i) a TWM pump with a spatially continuous wave of electric potential applied on a boundary (we call it a "single-mode arrangement"), (ii) a TWM pump with a wave of electric potential applied on a set of discrete electrodes, and (iii) a 3DM pump. The first approach is based on the use of the capacitor–resistor boundary condition for electric potential and the slip boundary condition for velocity. The other approach uses a non-equilibrium mathematical model based on the Poisson equation. The main motivation of the presented work is to verify the predictions reported in [13, 19] and to clearly show limitations of the capacitor–resistor approach.

2 Mathematical models

2.1 Micropump configurations

We consider four different arrangements of the AC electroosmotic pumps, Fig. 1. The micropumps are represented by a single segment of a long microfluidic channel. Each microchannel consists of an arbitrary large series of the segments. We assume that the microchannel width is much larger than the characteristic dimensions of the segments, so the AC electroosmotic pumps can be described as two-dimensional objects ($x - y$ coordinates).

A symmetric water electrolyte is considered to be the fluid in microchannels. Symmetries of the charge numbers (mono-monovalent electrolyte) and the ion diffusivities (equal size of the anion and the cation) are assumed. For example, a solution of potassium chloride in pure water (pH 7) almost satisfies these conditions. Consideration of such symmetric electrolyte enables to eliminate phenomena that give rise to an increase of system complexity (effects of the diffusion potential, etc.). No changes of

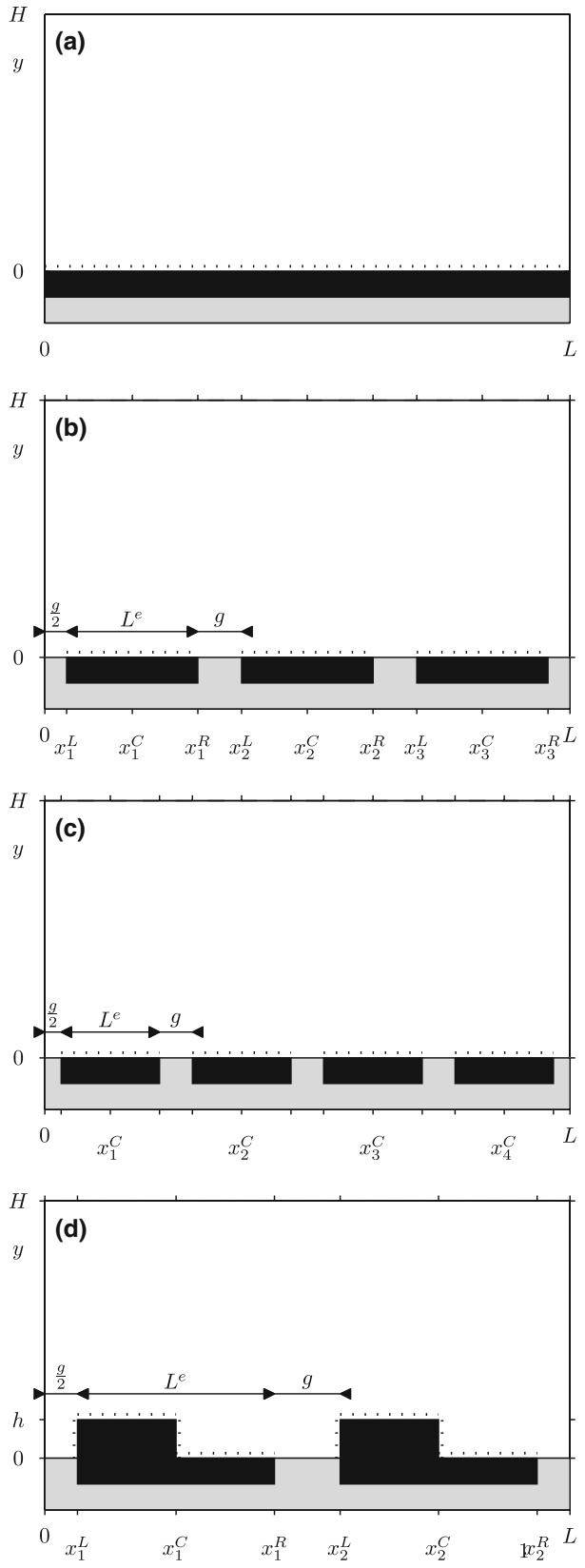

Fig. 1 Schematic configuration of the AC electroosmotic micropumps, **a** the single mode TWM system, **b** the three phase TWM system, **c** the four phase TWM system, and **d** the 3DM system

density, viscosity and temperature are expected. No faradaic reactions are assumed on the electrodes. Formation of the Stern part of EDL is not considered in this study.

The TWM pumps, Fig. 1a–c, are axially symmetric. Hence the transport processes are studied only in one half of the spatial domain. The single-mode TWM segment, Fig. 1a, can be characterized by the half-height H and the length L. The three and four TWM arrangements, Fig. 1b, c, are described by the half-height H, the length L, the electrode length L^e, and the length of the gap between adjacent electrodes g. The 3DM system is not axially symmetric and is represented by four geometric characteristics: the segment height H and length L, the electrode width L^e, the length of the gap between adjacent electrodes g, and the height of the electrode step h.

The electric potential on the electrodes is a known function of space and time defined for the single-mode TWM arrangement by

$$\varphi^e(x,t) = A\cos(\omega t - kx) = \Re(\psi^e \exp(i\omega t)), \tag{1}$$

$$\psi^e(x) = A\exp(-ikx), \quad x \in (0,L), \quad k = 2\pi/L \tag{2}$$

and for the other arrangements by

$$\varphi^e_m(t) = \varphi^e\left(x^C_m, t\right) = \Re\left(\psi^e_m \exp(i\omega t)\right), \tag{3}$$

$$\psi^e_m = A\exp\left(-ikx^C_m\right), \tag{4}$$

where

$$x^C_m = L(m-0.5)/n, \quad m = 1,2,\ldots,n. \tag{5}$$

is the position of the center of the m-th electrode in a n electrode system.

2.2 Non-equilibrium approach

The electric potential field satisfies the Poisson equation

$$\varepsilon\nabla^2\varphi = -q, \quad q = F(c^+ - c^-). \tag{6}$$

In order to evaluate the field of electric charge density, two molar balances for the anion $(-)$ and the cation $(+)$ have to be used

$$\frac{\partial c^\pm}{\partial t} = -\nabla\cdot\mathbf{J}^\pm. \tag{7}$$

The total molar flux density of ions is given by the sum of the convective and electromigration-diffusion contributions (the Nernst–Planck equation)

$$\mathbf{J}^\pm = \mathbf{v}c^\pm - D\left(\nabla c^\pm \pm c^\pm \frac{F}{RT}\nabla\varphi\right). \tag{8}$$

The velocity and pressure fields in the electrolyte are described by the Navier–Stokes equation and the continuity equation for incompressible Newtonian fluids

$$\rho\left(\frac{\partial \mathbf{v}}{\partial t}+\mathbf{v}\cdot\nabla\mathbf{v}\right)=\eta\nabla^2\mathbf{v}-\nabla p-q\nabla\varphi, \tag{9}$$

$$\nabla\cdot\mathbf{v}=0. \tag{10}$$

The non-slip boundary conditions are used on the electrolyte-solid interfaces

$$\mathbf{v}=0. \tag{11}$$

The Dirichlet boundary conditions are used for electric potential on the continuous electrode (the single-mode TWM)

$$\varphi^e=\varphi^e(x,t),\quad x\in(0,L), \tag{12}$$

or on the discrete electrodes

$$\varphi^e=\varphi^e_m(t),\quad x\in\left(x^L_m,x^R_m\right),\quad m=1,\ldots,n. \tag{13}$$

No Faradaic current through the solid-electrolyte interfaces is considered

$$\mathbf{n}\cdot\mathbf{J}^{\pm}=0. \tag{14}$$

The insulating boundary conditions are used for electric potential on the non-electrode solid boundaries

$$\mathbf{n}\cdot\nabla\varphi=0. \tag{15}$$

Periodical boundary conditions at $x=0$ and $x=L$ are applied

$$\boldsymbol{\xi}(x,y,t)=\boldsymbol{\xi}(x+L,y,t),\quad \boldsymbol{\xi}=\varphi,\mathbf{v},p,c^{\pm}. \tag{16}$$

At $y=H$ we use either the condition of the planar symmetry (TWM system) or a solid wall (3DM system). In order to obtain consistent set of hydrodynamic conditions, we define value of the reference pressure in one arbitrary point.

2.3 Equilibrium approach

The equilibrium approach enables to decouple the entire problem to the electrostatic and flow parts.

The electrical problem in the electrolyte bulk is governed by the Laplace equation due to the electroneutrality assumption

$$\nabla^2\varphi=0. \tag{17}$$

The boundary conditions for electric potential are the same as in the non-equilibrium model except the electrode boundaries. Here the capacitor–resistor boundary conditions are used [31, 32]

$$\mathbf{n}\cdot\sigma\nabla\varphi=-C_D\frac{\partial}{\partial t}(\varphi^e-\varphi). \tag{18}$$

Electric potential on the continuous electrode and the discrete electrodes is described by Eqs. 12 and 13, respectively.

Using complex formulation

$$\varphi(x,y,t)=\Re[\psi(x,y)\exp(i\omega t)], \tag{19}$$

where ψ is a complex function expressing the time-independent part of the potential field, we can rewrite Eqs. 17 and 18 in to the form

$$\nabla^2\psi=0, \tag{20}$$

$$\mathbf{n}\cdot\sigma\nabla\psi=-i\omega C_D(\psi^e-\psi), \tag{21}$$

where for the continuous electrode

$$\psi^e=\psi^e(x),\quad x\in(0,L), \tag{22}$$

and for the discrete electrodes

$$\psi^e=\psi^e_m,\quad x\in\left(x^L_m,x^R_m\right),\quad m=1,\ldots,n. \tag{23}$$

The Helmholtz–Smoluchowski equation describes the slip velocity on the outer boundary of EDL

$$\begin{aligned} v_{\text{slip}}&=\frac{\varepsilon}{\eta}(\varphi^e-\varphi)\mathbf{t}\cdot\nabla\varphi\\ &=\frac{\varepsilon}{\eta}\Re[(\psi^e-\psi)\exp(i\omega t)]\mathbf{t}\cdot\Re(\nabla\psi\exp(i\omega t)). \end{aligned} \tag{24}$$

The slip velocity represents the tangential velocity at EDL. The normal component of the velocity vector is considered to be zero at EDL.

The time averaged slip velocity can be expressed as

$$\begin{aligned} \hat{v}_{\text{slip}}&=\frac{1}{T_t}\int_t^{t+T_t}v_{\text{slip}}\mathrm{d}t\\ &=\frac{\varepsilon}{2\eta}\Re[(\psi^e-\psi)\mathbf{t}\cdot\nabla\psi^*]\\ &=\frac{\varepsilon}{2\eta}\Re(\psi^e-\psi)\mathbf{t}\cdot\Re(\nabla\psi)\\ &\quad+\frac{\varepsilon}{2\eta}\Im(\psi^e-\psi)\mathbf{t}\cdot\Im(\nabla\psi). \end{aligned} \tag{25}$$

The time averaged Stokes equation and the continuity equation are then used for description of the bulk hydrodynamics

$$0=\eta\nabla^2\hat{\mathbf{v}}-\nabla\hat{p},\quad \nabla\cdot\hat{\mathbf{v}}=0. \tag{26}$$

2.4 Dimensionless model

The model equations are transformed into a dimensionless form. We have used a similar scaling as in [33]. The spatial coordinates and the segment dimensions are scaled by the factor L

$$\begin{aligned} &\tilde{x}=\frac{x}{L},\quad \tilde{y}=\frac{y}{L},\quad \tilde{\nabla}=L\nabla,\quad \tilde{x}_m=\frac{x_m}{L},\quad \tilde{g}=\frac{g}{L},\\ &\tilde{h}=\frac{h}{L},\quad \tilde{H}=\frac{H}{L},\quad \tilde{L}^e=\frac{L^e}{L},\quad \tilde{\lambda}_D=\frac{\lambda_D}{L}. \end{aligned} \tag{27}$$

The dimensionless time $\tilde{t}$, the frequency $\tilde{f}$ and the angular frequency $\tilde{\omega}$ are given by

$$\tilde{t} = \frac{t}{t_\circ}, \quad t_\circ = \frac{\lambda_D L}{D}, \quad \lambda_D^2 = \frac{\varepsilon D}{\sigma} = \frac{\varepsilon RT}{2c_\circ F^2}, \\ \tilde{f} = f t_\circ, \quad \tilde{\omega} = \omega t_0 = 2\pi\tilde{f}. \tag{28}$$

The other dimensionless quantities are defined by

$$\tilde{q} = \frac{(c^+ - c^-)}{2c_\circ}, \quad \tilde{c} = \frac{c^+ + c^-}{2c_\circ}, \\ \tilde{\varphi} = \frac{\varphi}{\varphi_\circ}, \quad \varphi_\circ = \frac{RT}{F}, \quad \tilde{\psi} = \frac{\psi}{\varphi_\circ}, \quad \tilde{A} = \frac{A}{\varphi_\circ}, \\ \tilde{\mathbf{v}} = \frac{\mathbf{v}}{v_\circ}, \quad v_\circ = \frac{D}{L}, \quad \tilde{w} = \frac{w}{v_\circ} = \frac{\tilde{f}}{\tilde{\lambda}_D}. \\ \tilde{p} = \frac{p}{p_\circ}, \quad p_\circ = 2c_\circ RT. \tag{29}$$

A combination of Eqs. 6–10 and 27–29 gives the dimensionless form of the non-equilibrium mathematical model

$$\tilde{\nabla}^2\tilde{\varphi} = -\frac{1}{\tilde{\lambda}_D^2}\tilde{q}, \tag{30}$$

$$\frac{\partial\tilde{c}}{\partial\tilde{t}} = -\tilde{\lambda}_D\tilde{\nabla}\cdot\left(\tilde{\mathbf{v}}\tilde{c} - \tilde{\nabla}\tilde{c} - \tilde{q}\tilde{\nabla}\tilde{\varphi}\right), \tag{31}$$

$$\frac{\partial\tilde{q}}{\partial\tilde{t}} = -\tilde{\lambda}_D\tilde{\nabla}\cdot\left(\tilde{\mathbf{v}}\tilde{q} - \tilde{\nabla}\tilde{q} - \tilde{c}\tilde{\nabla}\tilde{\varphi}\right), \tag{32}$$

$$\frac{1}{\mathrm{Sc}}\left(\frac{\partial\tilde{\mathbf{v}}}{\partial\tilde{t}} + \tilde{\lambda}_D\tilde{\mathbf{v}}\cdot\tilde{\nabla}\tilde{\mathbf{v}}\right) \\ = \tilde{\lambda}_D\tilde{\nabla}^2\tilde{\mathbf{v}} + \frac{\mathrm{Ra}}{\tilde{\lambda}_D}\left(-\tilde{\nabla}\tilde{p} - \tilde{q}\tilde{\nabla}\tilde{\varphi}\right), \tag{33}$$

$$\tilde{\nabla}\cdot\tilde{\mathbf{v}} = 0. \tag{34}$$

The symbol $\tilde{\lambda}_D$ is a fundamental simplex given by the ratio of the Debye length λ_D (EDL thickness) and the geometric size of the system L. Except of the dimensionless Debye length, there are two other dimensionless parameters—the Schmidt and Rayleigh numbers. In this study, we do not deal with an asymptotic analysis of the model equation. Only results for a typical symmetric water electrolyte in microfluidic channels are reported. Hence in this section, the physical meaning of the dimensionless criteria is shortly discussed. Because the Schmidt number is high (particularly $\mathrm{Sc} = 500 \gg 1$), the concentration and electric charge boundary layers will be much thinner than the momentum boundary layers [34]. It means that the velocity field must be affected on a much higher distance from the electrodes than the concentration fields. Different behavior, not typical for microfluidic applications, can be expected for electrolytes with extremely low viscosities and with high diffusivities of ions. From the definition, the Rayleigh number expresses a ratio between the forces that destabilizes and stabilizes a static fluid [34]. In our modification, the dimensionless ratio $\mathrm{Ra}/\tilde{\lambda}_D^2$ is a relative ratio between the destabilizing electric body force and the stabilizing viscous force. This ratio is very high in the presented parametrical studies as well as in all AC microfluidic pumps. A low value of the ratio necessarily leads to zero net velocity.

The dimensionless form of the equilibrium model consist of the Laplace equation together with the capacitor–resistor boundary condition

$$\tilde{\nabla}^2\tilde{\psi} = 0, \tag{35}$$

$$\mathbf{n}\cdot\tilde{\nabla}\tilde{\psi} = -2\pi i\tilde{f}\left(\tilde{\psi}^e - \tilde{\psi}\right), \tag{36}$$

and the time averaged Stokes equation and continuity equation together with the slip boundary condition

$$0 = \tilde{\lambda}_D^2\tilde{\nabla}^2\hat{\tilde{\mathbf{v}}} - \tilde{\nabla}\hat{\tilde{p}}, \quad \tilde{\nabla}\cdot\hat{\tilde{\mathbf{v}}} = 0, \tag{37}$$

$$\mathbf{t}\cdot\hat{\tilde{\mathbf{v}}} = \hat{\tilde{v}}_{\mathrm{slip}} = \frac{\mathrm{Ra}}{2}\Re\left[\left(\tilde{\psi}^e - \tilde{\psi}\right)\mathbf{t}\cdot\tilde{\nabla}\tilde{\psi}^*\right], \tag{38}$$

The dimensionless electric potential on the electrodes in the single-mode TWM system is expressed as

$$\tilde{\psi}^e = \tilde{\psi}^e(\tilde{x}) = \tilde{A}\exp(-2\pi i\tilde{x}), \tag{39}$$

and in the discrete electrode TWM systems

$$\tilde{\psi}^e = \tilde{\psi}^e_m = \tilde{A}\exp\left(-2\pi i\tilde{x}^C_m\right), \\ x^C_m = \frac{m - 0.5}{n}, \quad m = 1, 2, \ldots, n. \tag{40}$$

For the single-mode TWM system, Ramos et al. [19] pointed an analytical solution of (35) and (36)

$$\tilde{\psi} = \tilde{A}\frac{i\tilde{f}}{1 + i\tilde{f}}\exp(-2\pi i\tilde{x} + 2\pi\tilde{y}). \tag{41}$$

Substituting (41) and (39) into (38) we obtain

$$\langle\tilde{v}\rangle = \hat{\tilde{v}}_{\mathrm{slip}} = \mathrm{Ra}\frac{\pi\tilde{f}}{1 + \tilde{f}^2}\tilde{A}^2. \tag{42}$$

In this case, the time averaged slip velocity does not depend on the x-coordinate and then is equal to the net velocity.

3 Numerical analysis

3.1 Solvers

Numerical analyses both of the non-equilibrium and the equilibrium models were carried out in the Comsol Multiphysics software.

We used a standard *femtime* procedure for the dynamical analysis of the non-equilibrium mathematical model, Eqs. 30–34 and the boundary condition (11–16) in the

dimensionless form. Transient simulations from a homogeneous steady state to stable periodic regimes were carried out in the first step. The obtained stable period solutions were then analyzed to compute the time-averaged net velocity and other characteristics of the AC electroosmotic flow.

The model equations describing the non-equilibrium TWM system were alternatively analyzed using a nonlinear stationary solver *femnlin* after a transformation to moving coordinates.

The numeric analysis of the equilibrium model (35, 37) with boundary conditions (36, 38) was realized in two steps. The analysis of the linear electric potential problem (35, 36) for the discrete electrode systems was done using a linear *femnlin* solver in the first step. The flow problem (37, 38) was solved by the *femnlin* solver.

3.2 Spatial discretization

The Comsol Multiphysics software requires discretization of spatial domains into a set of finite elements. Parameters of the element meshes depend on the type of the AC electroosmotic pumps. As an example, we mention mesh parameters of the 3DM system. In the non-equilibrium model, we always used hybrid triangle-rectangle meshes of finite elements, which enables efficiently discretize the entire spatial domain including EDLs, Fig. 2a. The rectangle elements with a high aspect ratio (up to $6.7 \times 10^{+3}$) were employed in EDLs, whereas the triangle elements were used at electrode edges and in the electrolyte bulk. The edge size of the smallest and the largest elements was 1.2×10^{-6} and 8×10^{-2} dimensionless units, respectively. Meshes of the triangle finite elements were employed in the equilibrium 3DM model, Fig. 2b. Higher element densities were used at the electrode edges. The edge size of the smallest and the largest elements was 1×10^{-4} and 1×10^{-1} dimensionless units, respectively. Number of the finite elements was approximately equal to 7000 and 4500 for the non-equilibrium and equilibrium models, respectively. As an improper spatial discretization can result in an unacceptable error of the numerical approximation, meshes of various structures and densities were tested.

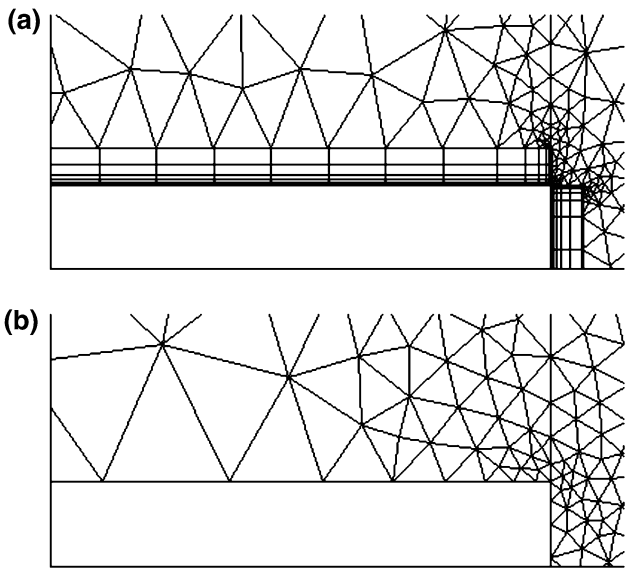

Fig. 2 Examples of meshes used for the 3DM arrangement, **a** non-equilibrium model, **b** equilibrium model. Only details above electrode edges are plotted, detail size: 0.08×0.03 dimensionless units

4 Results and discussion

Selected dependencies of the net velocity on principal model parameters such as the dimensionless frequency, the dimensionless amplitude or the dimensionless step height (3DM system) are presented in this section. Results obtained by analyses of the non-equilibrium and the equilibrium models are compared. The detected discrepancies and their possible origins are discussed. In Figs. 3, 4, 5, 6, 9, 10, 11, 12 and 13, parametric dependencies computed by the non-equilibrium model are plotted by dashed lines with empty markers. The equilibrium results are represented by solid lines with filled markers. The solid lines without markers denote the velocity of the electric potential traveling wave.

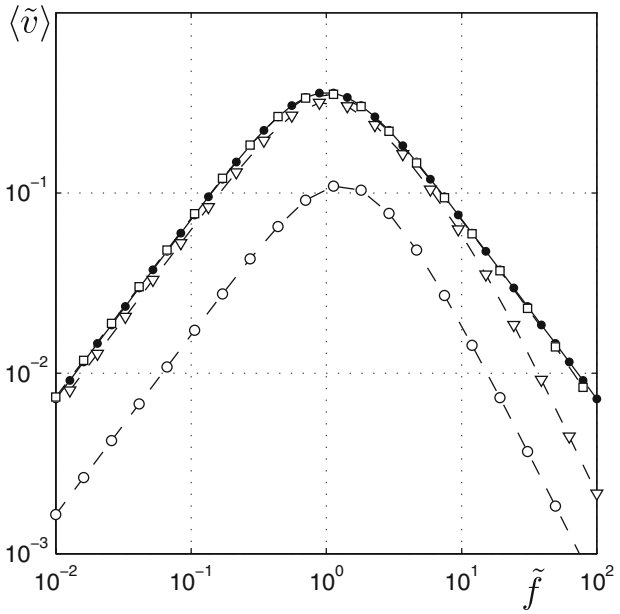

Fig. 3 Dependencies of the dimensionless velocity on the dimensionless frequency for the single mode TWM system, $\tilde{\lambda}_D = 0.1$—*circle*, $\tilde{\lambda}_D = 0.01$—*triangle* and $\tilde{\lambda}_D = 0.001$—*square*. *Solid* (*empty*) markers represents the equilibrium (non-equilibrium) model. Dimensionless amplitude: $\tilde{A} = 1$

4.1 Single mode traveling wave pump

First of all, we present results of the parametric study for the single mode traveling wave arrangement. Solution of the equilibrium model is given by Eq. 42. Non-equilibrium solutions are obtained numerically.

4.1.1 Frequency and amplitude characteristics

Dependencies of the net velocity on the AC frequency are shown in Figs. 3, 4, 5 and 6. In the logarithmic plot, these dependencies are concave functions with a single maximum that can be found at $\tilde{f} \approx 1$. It reflects a conclusion of the capacitor–resistor theory that predicts the maximal net velocity for the frequency $D/(L\ \lambda_D)$ [20].

Effects of the ratio of the EDL thickness and the segment length ($\tilde{\lambda}_D$) for low amplitude regimes ($\tilde{A} = 1$) are demonstrated in Fig. 3. Because for such low amplitudes the EDL capacitance is constant (the linearization used by the equilibrium model is justified), one can expect quantitative agreement between the prediction of the equilibrium and the non-equilibrium models. However, it is shown that the frequency dependencies predicted by both the models coincide only for very low values of $\tilde{\lambda}_D$. If the parameter $\tilde{\lambda}_D$ is equal to 0.1, clouds of electric charge penetrate far from the electrode and the EDL domain can not be further neglected when the flow problem is solved. The non-equilibrium model predicts a substantial decrease of the net velocity in such case. One of the equilibrium model assumptions is that the EDL thickness is negligible. However, no quantitative measure of this "negligibility" is given. The results plotted in Fig. 3 clearly demonstrate validity of the thin EDL assumption in the meaning of the dimensionless Debye length in the TWM system.

Slopes of the net velocity characteristics predicted by both the models can differ for $\tilde{f} > 1$, see Figs. 4, 5 and 6. The AC frequency, for which this difference becomes significant, depends on the dimensionless Debye length. If Figs. 4, 5 and 6 are compared, it can be seen that for a smaller Debye length the slopes deviates at higher frequencies. The observed effect is related to the EDL relaxation. There are at least two important time scales. From the RC circuit theory, the maximal signal gain is obtained when the period of an AC electric field is approximately equal to the charging time $L\lambda_D/D$. However, EDL can be in the thermal equilibrium on a shorter time scale that is equal to the characteristic diffusion Debye time (Debye time) of ions across EDL λ_D^2/D [20]. If the AC frequency is higher than the reciprocal diffusion time, the electric charge distribution in EDLs must be highly deviated from the Boltzmann distribution. It happens for the dimensionless frequencies higher than $\tilde{\lambda}_D^{-1}$.

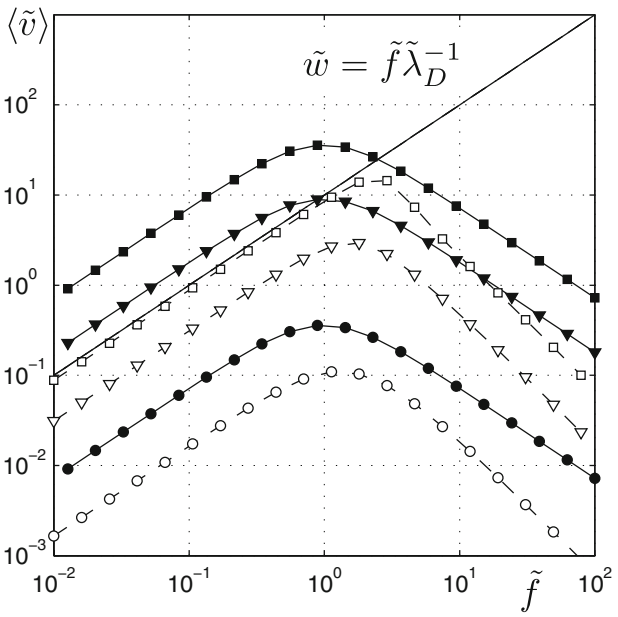

Fig. 4 Dependencies of the dimensionless velocity on the dimensionless frequency for the single mode TWM system, $\tilde{A} = 1$—*circle*, $\tilde{A} = 5$—*triangle* and $\tilde{A} = 10$—*square*. *Solid* (*empty*) markers represent the equilibrium (non-equilibrium) model. System size: $\tilde{\lambda}_D = 0.1$

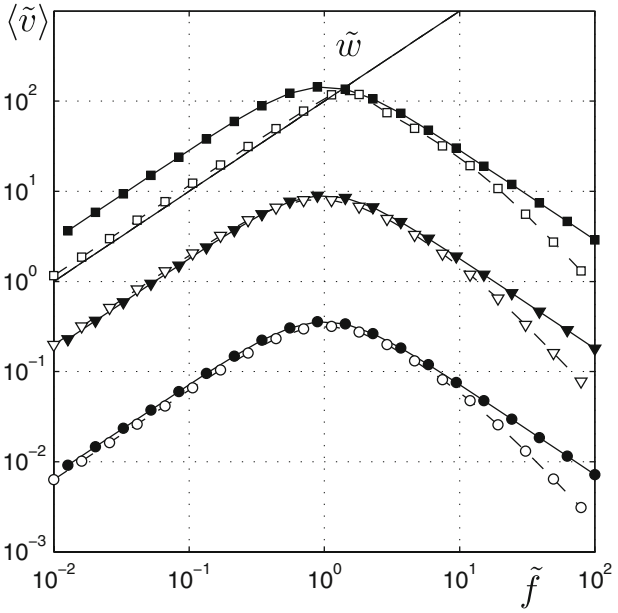

Fig. 5 Dependencies of the dimensionless velocity on the dimensionless frequency for the single mode TWM system, $\tilde{A} = 1$—*circle*, $\tilde{A} = 5$—*triangle* and $\tilde{A} = 20$—*square*. *Solid* (*empty*) markers represent the equilibrium (non-equilibrium) model. System size: $\tilde{\lambda}_D = 0.01$

The time averaged net velocities obtained by the mathematical models are compared with the velocity of the traveling wave electric potential (solid line), Figs. 4, 5 and 6. If $\tilde{\lambda}_D$ is high (e.g., thin channels filled with a low concentrated electrolyte), the equilibrium model predicts much

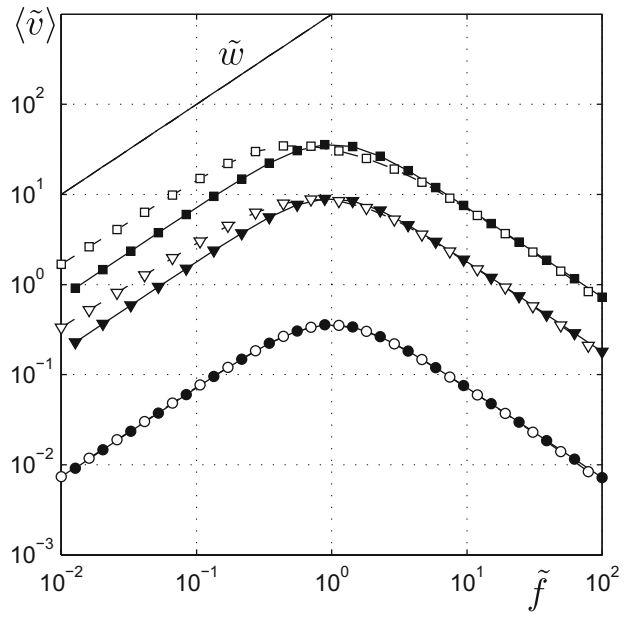

Fig. 6 Dependencies of the dimensionless velocity on the dimensionless frequency for the single mode TWM system, $\tilde{A} = 1$—*circle*, $\tilde{A} = 5$—*triangle* and $\tilde{A} = 10$—*square*. *Solid* (*empty*) markers represent the equilibrium (non-equilibrium) model. System size: $\tilde{\lambda}_D = 0.001$

higher net velocities than the non-equilibrium model, Fig. 4. The net velocity computed by the equilibrium model surprisingly exceeds the velocity of the electric potential wave $\tilde{w} = \tilde{f}\tilde{\lambda}_D^{-1}$ for higher amplitudes $\tilde{A}$ and smaller frequencies $\tilde{f} < 1$.

Of course, this unphysical prediction is given by the limitations of the equilibrium model (the Debye length thickness and the linearization limit). Conversely, the non-equilibrium model produces physically relevant data. The non-equilibrium results for $\tilde{A} = 10$ and $\tilde{f} < 1$ almost coincide with the electric potential wave velocity and the net velocity never exceed the electric potential wave limit.

For $\tilde{\lambda}_D = 0.01$, Fig. 5, the predictions of both the models are in relatively good agreement in low amplitude regimes ($\tilde{A} = 1$ or $\tilde{A} = 5$). The equilibrium model predictions are more reliable in such regimes due to a smaller Debye layer thickness. Thus the frequency and amplitude influences on behavior of the TWM electroosmotic pump can be clearly observed. As the AC frequency approaches the reciprocal Debye time, slopes of the velocity characteristics predicted by both the models become different because the equilibrium model does not describe EDLs out of the thermal equilibrium. The amplitude limitation of the equilibrium model is distinctly visible in the high amplitude regime $\tilde{A} = 20$, when the estimated net velocity substantially exceeds the electric potential wave velocity. The velocity predicted by the non-equilibrium model also slightly exceeds the electric potential wave velocity $\tilde{w}$ in this regime. The most probable reason for this behavior is given by a limited precision of numerical approximations.

To estimate the numerical errors caused by the spatial discretization, we carried out convergence studies in selected points of the parametrical space. An example of such study is depicted in Fig. 7. In the TWM arrangement, meshes of the rectangle elements were equidistantly distributed along the x-axis. The distribution along the y-axis was always non-equidistant. The data in Fig. 7 show that the numerical errors resulting from the spatial discretization are negligible for the mesh setting usually used in the numerical analysis $n_{\mathrm{Fx}} \times n_{\mathrm{Fy}} = 60 \times 40$ (27 elements across EDL, the smallest edge size 9.2×10^{-5}). We should note that other numerical errors can result from the time discretization, the setting of the dynamical solver or the computation of mean values.

Differences between the equilibrium and non-equilibrium results occurring in low frequency regimes ($\tilde{f} < 1$) will be explained by means of Fig. 6. For high amplitudes, the maxima of the net velocities predicted by the non-equilibrium model are shifted to lower frequencies than those predicted by the other model. It results from the fact that the Debye layer capacitance is not constant above the

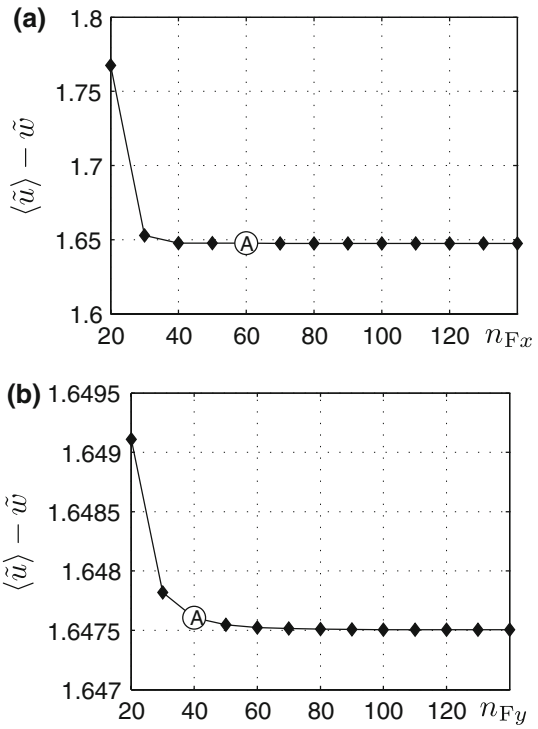

Fig. 7 Differences between the net velocity computed by the non-equilibrium model and the velocity of the electric potential wave are plotted as functions of the number of finite elements. **a** Dependence on the number of the discrete elements in the x-direction, $n_{\mathrm{Fy}} = 40$; **b** dependence on the number of the discrete elements in the y-direction, $n_{\mathrm{Fx}} = 60$; $\tilde{\lambda}_D = 0.01, \tilde{f} = 0.1, \tilde{A} = 20$. The marker *A* refers to the mesh setting used in parametric studies

linearization limit ($C_D > \varepsilon/\lambda_D$). The charging of a capacitor with a higher capacitance takes more time, i.e. the "optimal" charging frequency must be shifted to a lower value. This shift is clearly depicted in Fig. 6.

In low frequency and high amplitude regimes, the non-equilibrium model predicts higher net velocity than the equilibrium model, Fig. 6. Although, the EDL charging takes more time in a high amplitude regime, there is also an increase of the tangential component of the electric field strength, which finally results in the net velocity increase.

The above described phenomenon can be compensated or overcome by another effect in the cases presented in Figs. 4 and 5. As the net velocity approaches the velocity of the electric potential wave, hydrodynamic limitations become important. In the equilibrium model, the net velocity at a fixed frequency can grow to infinity with increasing amplitude (it results from Eq. 24). However, the net velocity is physically limited by the velocity of the electric potential wave that pulls clouds of the formed electric charge. The pulled ions interact with the liquid by viscous forces, which then results in the net flow. This behavior is well described by the non-equilibrium model. The hydrodynamic flow must be necessarily delayed with respect to the electric potential wave propagation.

4.1.2 Dynamical fields

As an illustrative example, we show the evolution of a velocity field computed by the non-equilibrium model for the three-electrode TWM pump, Fig. 8. The velocity patterns are plotted in selected phases of the stable periodic regime, i.e. after the initial transient. Typical eddies are formed at the electrode edges. Two periods of the velocity pattern can be easily identified. The first one results from the fact that a change of the electrode polarity has no effect on the direction both of the coulombic force and the net velocity. Hence this period is equal to one half of the electric field period (180°). The other period is given by the voltage phase shift between adjacent electrodes. In the three electrode arrangement, we can observe the same pattern after each one sixth of the voltage period (60°). After each 60°, the velocity pattern moves over one third of the segment length to the right. This space shift equivalently corresponds to the pattern move over one third of the segment length to the left after each 120°.

4.2 Discrete electrodes

It is difficult to construct an experimental single mode TWM pump. Instead of it, the single mode TWM systems can be approximated by a set of discrete planar electrodes among them a voltage phase shift is applied. In Fig. 9, dependencies of the net velocity on the AC frequency for

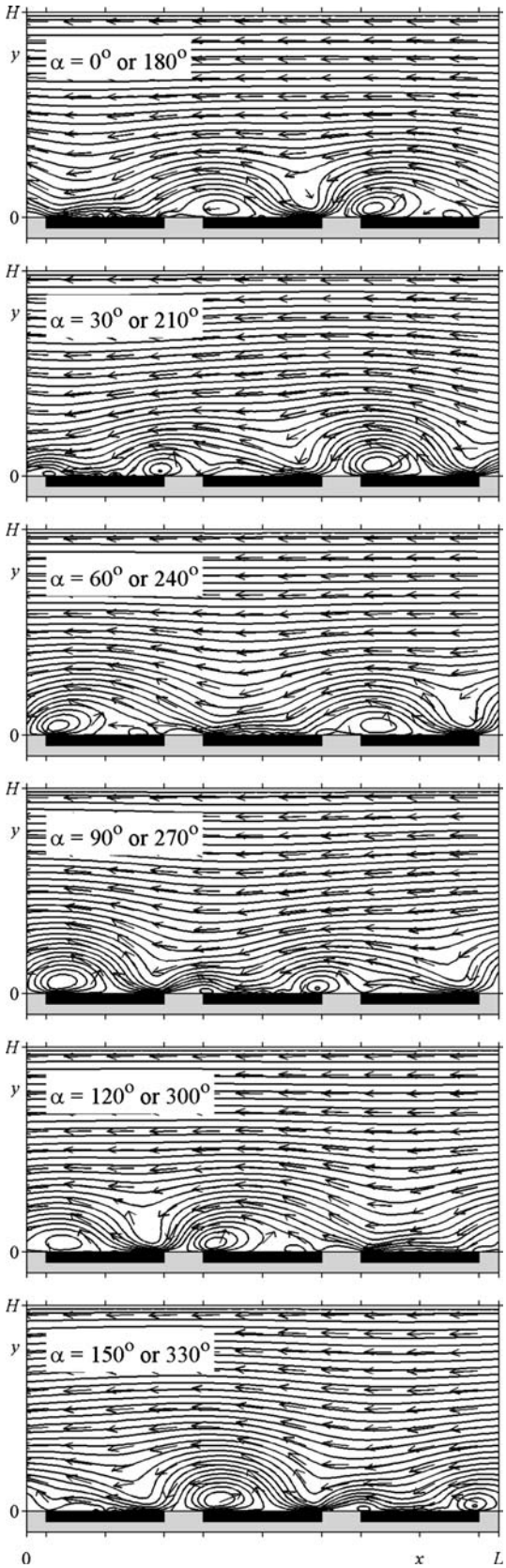

Fig. 8 The velocity field in various phases of the applied electric signal α. Non-equilibrium model, $\tilde{\lambda}_D = 8.333\times10^{-4}$, $\tilde{A} = 10$, $\tilde{f} = 1.2$

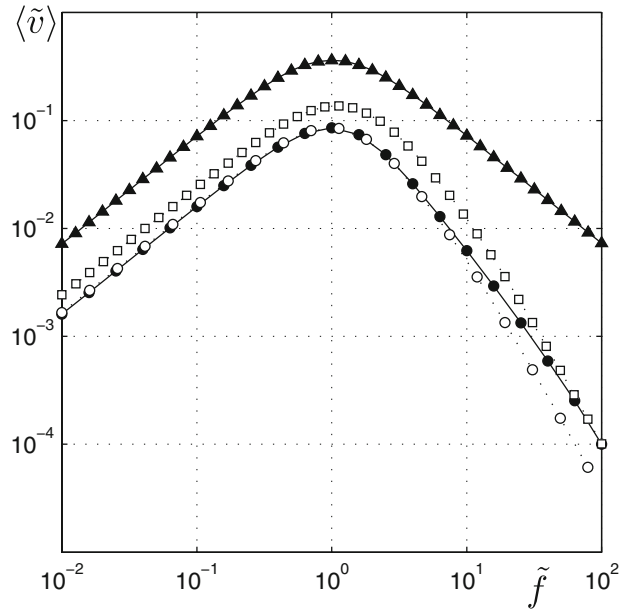

Fig. 9 Dependencies of the dimensionless velocity on the dimensionless frequency. Equilibrium single mode TWM system—*solid triangles*, non-equilibrium four electrode TWM system—*empty squares*, non-equilibrium three electrode TWM system—*empty circles*, equilibrium three electrode TWM system—*solid circles*. Dimensionless amplitude: $\tilde{A} = 1$. System size: $\tilde{\lambda}_D = 0.001$

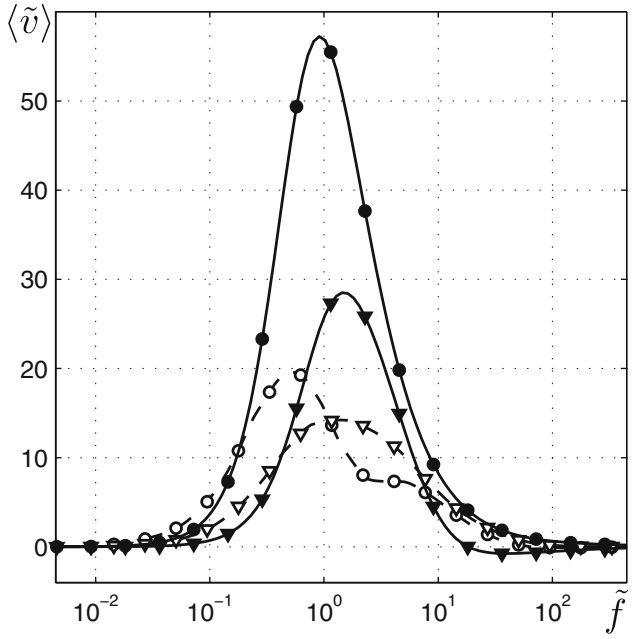

Fig. 10 Dependencies of the dimensionless velocity on the dimensionless frequency for the 3DM system, $\tilde{\lambda}_D = 3.647 \times 10^{-3}$, $\tilde{A} = 56.15$. $\tilde{h} = 0.02$—*triangle*, $\tilde{h} = 0.1$—*circle*. *Solid* (*empty*) markers represent the equilibrium (non-equilibrium) model

the single mode, three-electrode and four-electrode arrangements are plotted. The net velocities obtained for the discrete electrode TWM systems are always smaller than those for the single mode TWM system. In the discrete systems, the microchannel surface is polarized only at the electrodes. Hence the coulombic force is localized especially at the electrode [9] and does not induce the electroosmotic flow along the entire spatial domain. One can see that the net velocity predicted for four-electrode arrangement is higher than that for the three-electrode arrangement. It is because the four-electrode arrangement better approximates the single-mode system. Further, results given by the equilibrium and the non-equilibrium models for the three-electrode arrangement were compared. The obtained velocity dependencies almost coincide for the selected set of parameters. Discrepancies are observed only in high-frequency regimes, in which the Boltzmann distribution is not satisfied.

4.3 Non-planar electrodes

4.3.1 Frequency and amplitude characteristics

The frequency dependencies of the net velocity for the 3DM system are plotted in Fig. 10. All velocity maxima are located close to $\tilde{f} = 1$. It agrees with the prediction of the RC circuit theory [20]. However, there are two significant discrepancies between the equilibrium and the non-equilibrium results. The non-equilibrium model predicts smaller net velocities for $\tilde{f} = 1$ than the other model. If the net velocity is transformed back to the dimensional form, the non-equilibrium results are much closer to the experimental data reported in [12, 13]. This result can be expected because the linearization used in the equilibrium model is not justified for the system where $\tilde{A} \gg 1$.

Further, the non-equilibrium velocity dependence for $\tilde{h} = 0.1$ has not a single peak shape. It looks more like two merged peaks. Two peak patterns were experimentally observed by Urbanski et al. (see Fig. 4 in [12]) but not predicted by the equilibrium model [13]. The presence of the two-peak patterns probably results from the fact that there are more than one geometric length scale in the 3DM arrangement. Only one geometric scale L is usually used, however, the step height h at least partially represents another geometric scale. By other words, the characteristic length of the resistor domain is affected both by the length of the segment and the electrode step height. These two geometric scales typically differ by one order of magnitude, which corresponds with the distance between the two velocity maxima in the frequency characteristics, dashed line in Fig. 10 and [12].

For a complex view on the 3DM problem, the frequency characteristic in a low amplitude regime is plotted in Fig. 11. The model predictions are in a relatively good agreement for $\tilde{f} < 1$ and both the net velocity maxima are

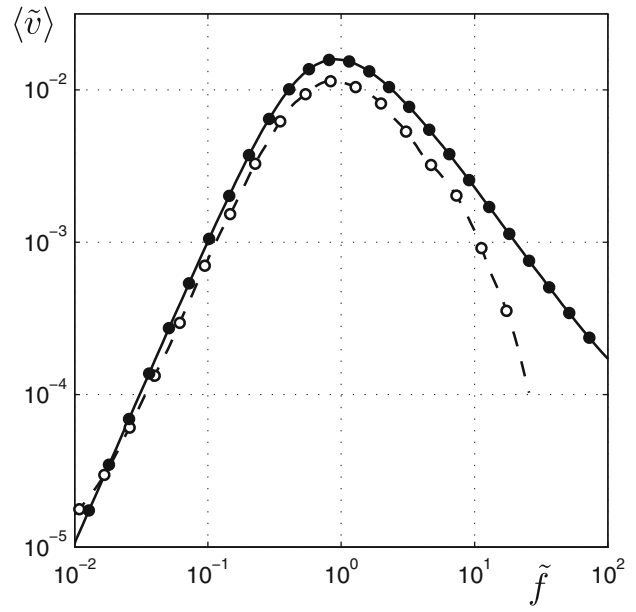

Fig. 11 Dependencies of the dimensionless velocity on the dimensionless frequency for the 3DM system, $\tilde{\lambda}_D = 3.647 \times 10^3, \tilde{A} = 1, \tilde{h} = 0.1$. *Solid* (*empty*) markers represent the equilibrium (non-equilibrium) model

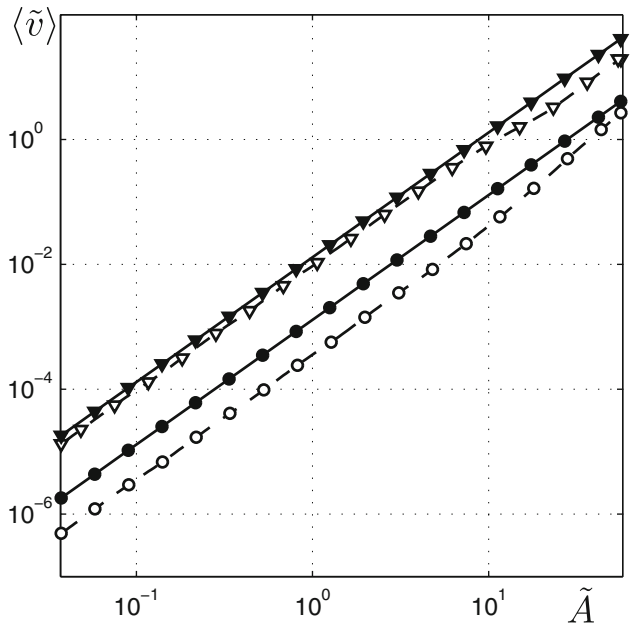

Fig. 12 Dependencies of the dimensionless velocity on the amplitude for the 3DM system, $\tilde{\lambda}_D = 3.647 \times 10^{-3}, \tilde{h} = 0.1$. $\tilde{f} = 0.4559$—*triangle*, $\tilde{f} = 18.23$—*circle*. *Solid* (*empty*) markers represent the equilibrium (non-equilibrium) model

again found at $\tilde{f} = 1$. The velocity characteristic diverges especially for $\tilde{f} > 10$. The existence of the two length scales of the resistor domain is the most probable reason for such behavior. The ratio between the charging frequency for the resistor domain of length h (the step size) and L (the segment length) is given by the reciprocal dimensionless step height $\tilde{h}^{-1}$. There are at least two reasons why the net velocity predicted by the non-equilibrium models is usually smaller in the studied frequency range. At the electrode corners, EDLs are not one-dimensional even if their thickness is small. Further, if the equilibrium model is used, velocity discontinuities are applied on the corners, which can possibly result in an unpredictable behavior.

The velocity dependencies on the amplitude were also computed, Fig. 12. According to the theory [1], the velocity predicted by the equilibrium model is proportional to the amplitude square. The same is true for the non-equilibrium model up to $\tilde{A} \approx 5$. The non-equilibrium dependencies become non-linear for higher amplitudes. The ratio between the net velocities predicted by the equilibrium and the non-equilibrium models remains constant in low amplitude regimes. The dependencies almost coincide for $\tilde{f} = 0.4559$, however, a higher discrepancy is observed for the other frequency, $\tilde{f} = 18.23$. When a higher frequency is applied, the EDL has a more dynamical character. In the meaning of the equilibrium model, the capacitor thickness is not given by the Debye length.

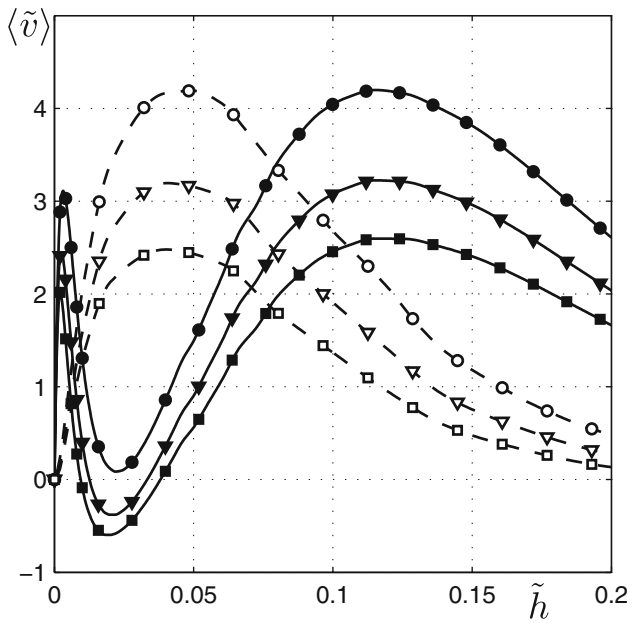

Fig. 13 Dependencies of the dimensionless velocity on the electrode step height for the 3DM system, $\tilde{\lambda}_D = 3.647 \times 10^{-3}, \tilde{A} = 56.15$. $\tilde{f} = 18.23$—*circle*, $\tilde{f} = 22.79$—*triangle*, $\tilde{f} = 27.35$—*square*. *Solid* (*empty*) markers represent the equilibrium (non-equilibrium) model

4.3.2 Step-size characteristics

Dependencies of the net velocity on the electrode step size for three different frequencies are shown in Fig. 13. We have compared these characteristics with experimental

results published in [12]. The maximal net velocities predicted by both the models are comparable with the experimental data. The non-equilibrium model does not predict the flow reversals that were experimentally observed for low electrode step sizes (for given set of parameters). However, the non-equilibrium model is able to better sense the positions of the velocity maxima and the velocity decrease for higher step sizes. If compared with the experimental data (Fig. 9 in [12]), the equilibrium model underestimates the net velocity for low step sizes and overestimates it for high step sizes. Moreover, the velocity characteristics obtained by the equilibrium model are characterized by two local maxima. The maximum observed for very low step sizes is unexpected and physically unjustified. We suggest the following reason for these discrepancies. In the 3DM arrangement, the formed EDL is truly two-dimensional. Clouds of the electric charge that temporarily accumulates above the horizontal and the vertical electrode surfaces necessarily overlap. The concept of the slip velocity especially at the electrode corners leads to physical and also numerical difficulties.

5 Conclusions

We have compared the equilibrium and non-equilibrium approaches for mathematical modeling of AC electroosmotic micro and nanosystems. We have found that there are many discrepancies between the model predictions. The equilibrium model is, of course, a rougher approximation of real physical systems. Hence, the discrepancies were expected in regimes where the equilibrium model assumptions are not satisfied. Several reasons for the observed discrepancies have been identified: (I) non-constant EDL capacitance in high amplitude regimes, (II) the slip boundary conditions do not respect a finite velocity of the applied electric potential wave in high amplitude regimes, (III) truly two-dimensional character of EDL, (IV) EDL can be out of the equilibrium, (V) a non-negligible EDL thickness, (VI) more spatial scales of the resistor domain (only the 3DM system), and (VII) the precision of numerical approximations. The comparison of the equilibrium and non-equilibrium results has further shown three important actualities: (a) how the equilibrium model overestimates or underestimates the net velocity, (b) how the velocity maxima in the frequency characteristics can be shifted, if the equilibrium model assumptions are not satisfied, (c) a parametric region where the equilibrium model is applicable. Because the data are obtained in a dimensionless form, they can be used for various AC electroosmotic systems.

General conclusions can be expressed for the single mode TWM system. Predictions of the two models are in good agreement when the dimensionless Debye length is small (the $\tilde{\lambda}_D$ limit is between 0.001 and 0.01), the amplitude is small (the $\tilde{A}$ limit is between 1 and 5) and the frequency is lower than the reciprocal Debye time ($\tilde{f} > \tilde{\lambda}_D^{-1}$). A qualitative comparison with respect to the equilibrium model follows. If the frequency is higher than the reciprocal Debye time, the non-equilibrium model predicts smaller net velocities (reason IV). If the amplitude is higher than the limit and $\tilde{f} < 1$, the non-equilibrium model can predict higher (I) or smaller net velocities (II and/or V). When the $\tilde{\lambda}_D$ is above the limit, the net velocity from the non-equilibrium model is always lower (III–V). Further, the non-equilibrium model predicts shifts of the net velocity maximum to higher (reason II) and lower (reason I) frequencies than is the reciprocal charging time $L\,\lambda_D/D$.

The above described results can not be fully exploited in conclusions for the three and four electrode TWM systems and the 3DM systems due to additional geometric parameters. The numerical analysis of both the models showed that the attained net velocity in a discrete TWM system is always lower than in the single mode TWM system with the same characteristic parameters.

For certain parameter values, the dependence of the net velocity on the AC frequency in the 3DM pumps is characterized by two local maxima [12]. Similar behavior indicates the non-equilibrium model. We assume that the two-peak frequency dependencies are given by two geometric scales of the resistor domain (VI). One of the scales must somehow depend on the height of the electrode step. We suggest identifying the other length scale and then modifying the equilibrium model in future. The two-dimensional character of EDL (III) should not be neglected if either EDLs overlap at electrode corners (3DM systems) or adjacent electrodes are so close that the EDLs merge (discrete TWM systems).

All numerically obtained results are necessarily deviated from exact solutions (VII). It is true for both the equilibrium model and the non-equilibrium model. Numerical errors result from the spatial and time discretizations, the evaluation of integral mean values (the net velocity) or variable discontinuities at domain boundaries (electric potential, the slip velocity). The presented numerical results were checked for selected sets of the model parameters. Hence, relative errors of the numerical approximations should not exceed an acceptable range.

It can be summarized that both the equilibrium and non-equilibrium models are powerful tools to design AC electroosmotic micropumps and to analyze their behavior. The obtained results are mostly similar if a voltage does not exceed the linearization limit. Hence the equilibrium model should be the first choice for a fast and qualitative analysis. However, for many cases, that are relevant to real experimental microdevices, the use of the equilibrium model is not justified. The non-equilibrium model should predict the

qualitative and the quantitative behavior of AC electroosmotic pumps more precisely in a much broader parameter range. But its implementation is difficult, more time consuming, and the results can be affected by a larger numerical error. For the future, we consider to carry out experimental measurement in well defined microchips in order to confirm or disprove the predictions of the non-equilibrium model. We must further note that the presented analysis does not consider the condensed layer formation [28–30].

We believe that the AC electroosmotic pumps could be promising tools for various microfluidic applications. This theoretical contribution presents an alternative non-equilibrium approach to predict their quantitative and qualitative behavior.

Acknowledgements The authors thank for the support by the grant of the GAAV ČR (KAN208240651), by the grant of the MŠMT ČR (MSM 6046137306), by the grant MPO ČR (Pokrok 1H-PK/24), and by the grant GAČR (GD 104/08/H055).

References

1. Ramos A, Morgan H, Green NG et al (1998) J Phys D 31:2338
2. Ajdari A (2000) Phys Rev E 61:R45
3. Campisi M, Accoto D, Dario P (2005) J Chem Phys 123:204724
4. Garcia-Sanchez P, Ramos A, Green G et al (2006) IEEE Trans Dielectr Electr Insul 13:670
5. Green NG, Ramos A, Gonzalez A et al (2002) Phys Rev E 66:026305
6. Mpholo M, Smith CG, Brown ABD (2003) Sens Actuators B 92:262
7. Studer V, Pepin A, Chen Y et al (2004) Analyst 129:944
8. Probstein RF (1994) Physicochemical hydrodynamics: an introduction. Wiley, New York
9. Green NG, Ramos A, Morgan H (2000) J Phys D 33:632
10. Bazant MZ, Ben YX (2006) Lab Chip 6:1455
11. Burch D, Bazant MZ (2008) Phys Rev E 77:055303(R)
12. Urbanski JP, Thorsen T, Levitan JA et al (2006) Appl Phys Lett 89:143508
13. Urbanski JP, Levitan JA, Burch DN et al (2007) J Colloid Interface Sci 309:332
14. Cahill BP, Heyderman LJ, Gobrecht J et al (2004) Phys Rev E 70:036305
15. Cahill BP, Heyderman LJ, Gobrecht J et al (2005) Sens Actuators B 110:157
16. Ramos A, Gonzalez A, Garcia-Sanchez P et al (2007) J Colloid Interface Sci 309:323
17. Ejsing L, Smistrup K, Pedersen CM et al (2006) Phys Rev E 73:037302
18. Mortensen NA, Olesen LH, Belmon L et al (2005) Phys Rev E 71:056306
19. Ramos A, Morgan H, Green NG et al (2005) J Appl Phys 97:084906
20. Squires TM, Bazant MZ (2004) J Fluid Mech 509:217
21. Olesen LH, Bruus H, Ajdari A (2006) Phys Rev E 73:056313
22. Kim BJ, Yoon SY, Sung H J et al (2007) J Appl Phys 102:074513
23. Loucaides N, Ramos A, Georghiou GE (2007) Microfluid Nanofluid 3:709
24. Khan T, Reppert PM (2005) J Colloid Interface Sci 290:574
25. Wang XM, Wu JK (2006) J Colloid Interface Sci 293:483
26. Pribyl M, Snita D, Marek M (2008) Multiphysical modeling of DC and AC electroosmosis in micro- and nanosystems. In: Petrone G, Cammarata G (eds) Recent advances in modelling and simulation. I-Tech Education and Publishing, Vienna
27. Cervenka P, Pribyl M, Snita D (2009) Microelectron Eng 86:1333
28. Kilic MS, Bazant MZ, Ajdari A (2007) Phys Rev E 75:021502
29. Kilic MS, Bazant MZ, Ajdari A (2007) Phys Rev E 75:021503
30. Storey BD, Edwards L R, Kilic MS et al (2008) Phys Rev E 77:036317
31. Levitan JA, Devasenathipathy S, Studer V et al (2005) Colloids Surf A 267:122
32. González A, Ramos A, Green NG et al (2000) Phys Rev E 61:4019
33. Postler T, Slouka Z, Svoboda M et al (2008) J Colloid Interface Sci 320:321
34. Deen WM (1998) Analysis of transport phenomena. Oxford University Press, New York